THE JOURNAL OF PHYSICAL CHEMISTRY C

Article

Cite This: J. Phys. Chem. C 2018, 122, 25948−25953

pubs.acs.org/JPCC

Effects of NO_2 Addition on the NH_3-SCR over Small-Pore Cu−SSZ-13 Zeolites with Varying Cu Loadings

Yulong Shan,[†,§] Xiaoyan Shi,[†,§] Guangzhi He,[†] Kuo Liu,[†,‡] Zidi Yan,[†,§] Yunbo Yu,[†,§,∥] and Hong He*[,†,§,∥]

[†]State Key Joint Laboratory of Environment Simulation and Pollution Control, Research Center for Eco-Environmental Sciences and [‡]Journal of Environmental Sciences Editorial Office, Research Center for Eco-Environmental Sciences, Chinese Academy of Sciences, 18 Shuangqing Road, Haidian District, Beijing 100085, China

[§]University of Chinese Academy of Sciences, Beijing 100049, China

[∥]Center for Excellence in Regional Atmospheric Environment, Institute of Urban Environment, Chinese Academy of Sciences, Xiamen 361021, China

ABSTRACT: Small-pore Cu−SSZ-13 zeolites with varying Cu loadings were applied in the standard and the fast selective catalytic reductions (SCR) of NO with NH_3. It was found that increased Cu loadings contributed to standard SCR, while inhibited fast SCR. The NO and NO_2 reaction pathways were analyzed under fast SCR conditions by comparing the NO and NO_2 conversion activities over Cu−SSZ-13 and H−SSZ-13 zeolites. At low temperatures, NO_2 addition strongly inhibited the NO conversion because of the formation of NH_4NO_3. Compared to medium- and large-pore zeolites, the small pores were blocked more severely by the formed NH_4NO_3, making it more difficult for the reactant molecules (NH_3 and NO_2) with geometric dimensions similar to those of the small pores to go through the channel opening. Additionally, at high temperatures when NH_4NO_3 decomposed, NO_2 showed a promotion effect on NO_x conversion because of the occurrence of the fast SCR reaction, especially on Cu−SSZ-13 with low Cu loadings.

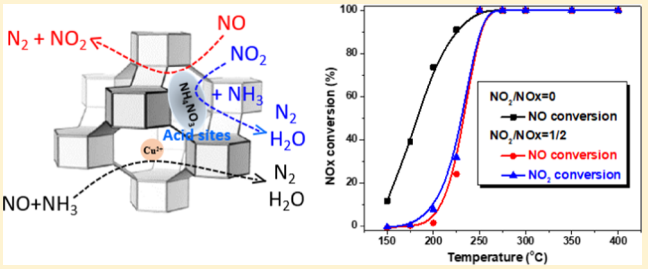

1. INTRODUCTION

The selective catalytic reduction of NO_x with NH_3 (NH_3-SCR) is an efficient technique for the abatement of NO_x from diesel engines. In recent years, copper-exchanged small-pore zeolites have been discovered to be efficient catalysts for NH_3-SCR because of their higher activity, N_2 selectivity, hydrothermal stability, and better resistance to hydrocarbons compared with the existing Cu−zeolite catalysts.[1−5] The fraction of NO in NO_x from diesel exhaust emissions is above 90 vol % in a real diesel exhaust. Therefore, the NH_3-SCR reaction, which is generally referred to as the standard SCR reaction involving equal amounts of NO and NH_3, occurs as shown in the following equation

$$4NH_3 + 4NO + O_2 \rightarrow 4N_2 + 6H_2O \quad (1)$$

Generally, the SCR performance is enhanced significantly when the NO_2 fraction in NO_x is increased to 50 vol %, which is the so-called "fast SCR" reaction involving the reaction of NH_3 with an equimolar mixture of NO and NO_2[6−13]

$$2NH_3 + NO + NO_2 \rightarrow 2N_2 + 3H_2O \quad (2)$$

The oxidation of NO to NO_2 has been suggested to be the rate-limiting step for the NH_3-SCR reaction.[14,15] However, Kwak et al. found that for Cu−SSZ-13 catalysts, NO oxidation was quite slow despite very high NO reduction activity.[16] They also found only a slight improvement in NO_x reduction over Cu−SSZ-13 under fast SCR conditions, which was an abnormal phenomenon since it is generally known that the addition of NO_2 to the feed is an effective way to achieve high SCR activity via the fast SCR reaction over catalysts such as V_2O_5−WO_3/TiO_2 and metal-exchanged zeolites at low temperatures.[6,17−19] In our previous work,[20] we found that the addition of NO_2 significantly decreased the NO_x conversion over the Cu−SSZ-13 catalyst with 3.9 wt % Cu loading because of the formation of NH_4NO_3, which blocked the zeolite pores. However, only one specified Cu loading (3.9 wt %) for Cu−SSZ-13 was studied in the work, and the effects of NO_2 addition over small-pore Cu−SSZ-13 zeolites with varying Cu loadings have not yet been fully explained. Additionally, the reason why medium- and large-pore zeolites (such as MFI and BEA) showed little or no inhibition by NO_2,[6,8,19,21] even though NH_4NO_3 accumulated on these zeolites, is unclear. In this work, the effects of NO_2 addition on NO_x conversion over Cu−SSZ-13 catalysts with varying Cu loadings were explored. By comparing the sizes of different types of zeolite pores and reactant molecules, the NH_4NO_3 inhibition mechanism on small-pore zeolites was uncovered.

Received: June 21, 2018
Revised: September 26, 2018
Published: October 29, 2018

DOI: 10.1021/acs.jpcc.8b05930
J. Phys. Chem. C 2018, 122, 25948−25953

2. EXPERIMENTAL SECTION

2.1. Catalyst Preparation. The initial Cu−SSZ-13 catalyst sample was synthesized using the one-pot synthesis method as reported previously.[22,23] The Cu loadings were adjusted to different levels by ion exchange using NH_4NO_3 solutions of varying concentrations. In detail, the initial Cu−SSZ-13 catalyst was ion-exchanged with 1 M NH_4NO_3 solution at 80 °C for 5 h to obtain the $Cu_{3.5}$−SSZ-13 catalyst. Then, the $Cu_{3.5}$−SSZ-13 catalyst was ion-exchanged with 0.05, 0.1, and 1.0 M NH_4NO_3 solutions at 40 °C for 5 h to obtain the $Cu_{2.4}$−SSZ-13, $Cu_{1.2}$−SSZ-13, and $Cu_{0.4}$−SSZ-13 catalysts, respectively. The ratio of the zeolite to solution was 1 g:100 mL. After the ion-exchange process, all samples were filtered, washed with distilled water, and dried at 100 °C overnight. Then, all catalyst samples were calcined in an oven at 600 °C for 6 h with a ramp rate of 5 °C/min. The concentrations of Cu reported here were obtained by inductively coupled plasma atomic emission spectroscopy (ICP-AES), and all samples are denoted as Cu_x−SSZ-13, where "x" represents the Cu content in the catalyst by weight (shown in Table 1).

Table 1. Cu, Si, Al Contents, Si/Al Ratios, and Cu/Al Ratios for the Samples

sample	Cu content (wt %)	Si/Al	Cu/Al	BET surface area (m^2/g)	micropore volume (cm^3/g)
$Cu_{3.5}$−SSZ-13	3.5	4.1	0.23	577.0	0.24
$Cu_{2.4}$−SSZ-13	2.4	4.6	0.16	565.9	0.23
$Cu_{1.2}$−SSZ-13	1.2	4.5	0.08	554.5	0.23
$Cu_{0.4}$−SSZ-13	0.4	4.6	0.03	602.5	0.25
H−SSZ-13	0	4.9	0	588.3	0.24

2.2. NH_3-SCR Activity Measurement. A fixed-bed quartz flow reactor was used to determine the catalyst activity at atmospheric pressure. About 50 mg samples of the catalyst (40−60 mesh) were evaluated, with a gas hourly space velocity (GHSV) of 400 000 h^{-1}. The reaction conditions were controlled as follows: $[NO_x] = [NO] + [NO_2] = 500$ ppm, $[NH_3] = 500$ ppm, $[O_2] = 5$ vol %, $[H_2O] = 5$ vol %, balance N_2, and total flow rate 500 mL/min. The NO, NO_2, NH_3, and N_2O concentrations were monitored by an online Nicolet Is10 spectrometer. The NO, NO_2, and NO_x conversions were calculated after recording the steady-state Fourier transform infrared spectra of the SCR reaction, and the equations were as follows

$$NO = \left(1 - \frac{[NO]_{out}}{[NO]_{in}}\right) \times 100\%$$

$$NO_2 = \left(1 - \frac{[NO_2]_{out}}{[NO_2]_{in}}\right) \times 100\%$$

$$NO_x = \left(1 - \frac{[NO]_{out} + [NO_2]_{out}}{[NO]_{in} + [NO_2]_{in}}\right) \times 100\%$$

2.3. Catalyst Characterization. The Cu loadings and Si/Al ratios of the samples were obtained by ICP-AES. A strong acid solution was used to dissolve the samples before testing. The Cu contents and Si/Al ratios are listed in Table 1. Powder X-ray diffraction (XRD) patterns were recorded on a computerized PANalytical X'Pert Pro diffractometer with Cu Kα (λ = 0.15406 nm) radiation. H_2 temperature-programmed reduction (TPR) in hydrogen was measured on a Micromeritics AutoChem 2920 chemisorption analyzer. The samples (~50 mg) were pretreated at 500 °C for 1 h with 20% O_2/N_2. After cooling down to ambient temperature, the samples were heated to 700 °C at a rate of 10 °C/min in 10% H_2/Ar gas flow. Temperature-programmed surface reaction (TPSR) experiments of the adsorbed NO_2 and NH_3 were performed in the NH_3-SCR activity measurement instrument. 30 mg samples of the catalysts pretreated in 20% O_2/N_2 for 1 h at 500 °C were put into an atmosphere of 500 ppm NO_2/N_2 after saturation by 500 ppm NH_3/N_2 at 150 °C, followed by N_2 purging for 1 h. Finally, the samples were heated to 600 °C in N_2 at a rate of 10 °C/min, and the production of N_2O was detected.

2.4. Calculations. To visually understand the shape selectivity of Cu−SSZ-13 zeolite toward the reaction gas molecules in the NH_3-SCR reactions, the molecular size of the reactants was defined by the electron density isosurface (isovalue = 0.0015 au),[24] and the molecular geometries of NH_3, NO, and NO_2 were calculated at the M06-2X/6-31G** level[25] with the Gaussian 09 package.[26] The electron density grid data were produced with the Multiwfn package.[27] The VMD software was used to visualize the geometries and the isosurface of electron density.[28]

3. RESULTS AND DISCUSSION

3.1. Physicochemical Characterization. The Cu−SSZ-13 catalysts with different Cu loadings were obtained by ion

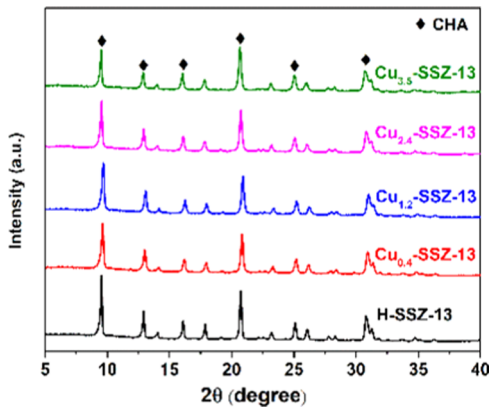

Figure 1. XRD patterns of the Cu−SSZ-13 and H−SSZ-13 zeolites.

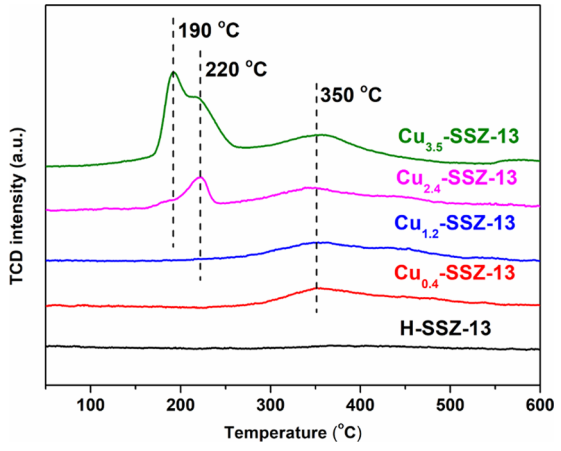

Figure 2. H_2-TPR profiles of the Cu−SSZ-13 and H−SSZ-13 zeolites.

DOI: 10.1021/acs.jpcc.8b05930
J. Phys. Chem. C 2018, 122, 25948−25953

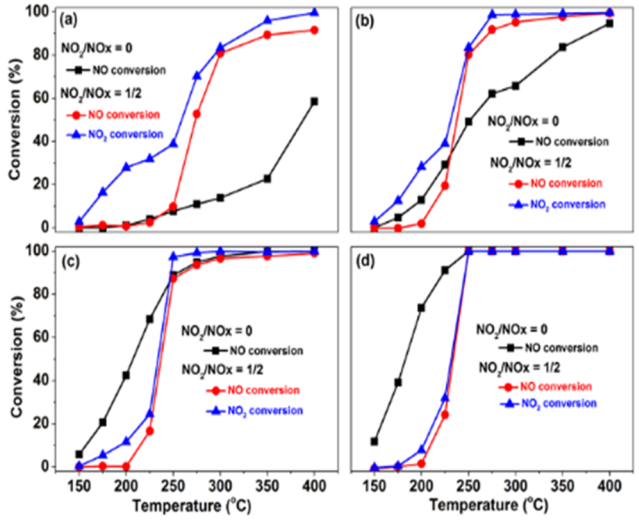

Figure 3. NH_3-SCR performances of (a) $Cu_{0.4}$−SSZ-13, (b) $Cu_{1.2}$−SSZ-13, (c) $Cu_{2.4}$−SSZ-13, and (d) $Cu_{3.5}$−SSZ-13. Conditions: NO_2/NO_x = 0: [NO] = [NH_3] = 500 ppm; NO_2/NO_x = 1:2: [NO] = [NO_2] = 250 ppm. [NH_3] = 500 ppm, 5 vol % H_2O, 5 vol % O_2, balance N_2, and GHSV = 400 000 h^{-1}.

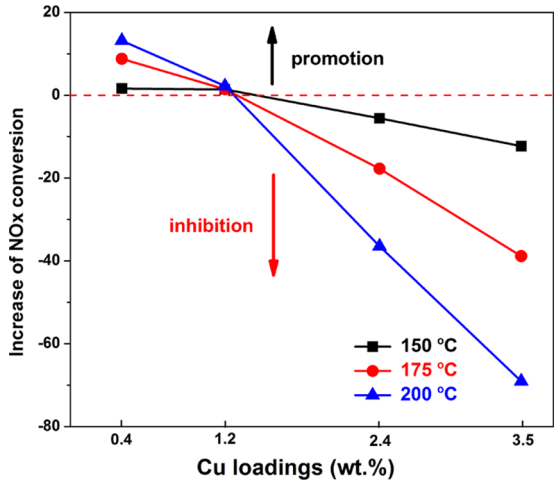

Figure 4. Increase of NO_x conversion as a function of Cu loadings under fast SCR conditions compared to that under standard SCR conditions. Increase of NO_x conversion = NO_x conversion (fast SCR) − NO_x conversion (standard SCR).

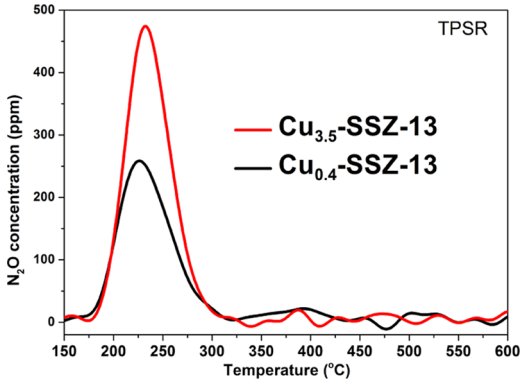

Figure 5. TPSR after NH_3 and NO_2 adsorption at 150 °C for $Cu_{3.5}$−SSZ-13 and $Cu_{0.4}$−SSZ-13. Adsorption conditions: [NO_2] = [NH_3] = 500 ppm.

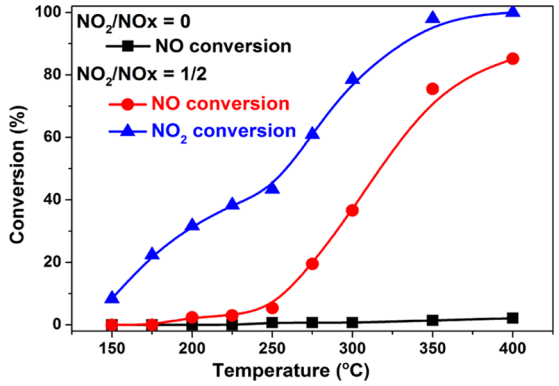

Figure 6. NH_3-SCR performance of H−SSZ-13. Conditions: NO_2/NO_x = 0: [NO] = [NH_3] = 500 ppm; NO_2/NO_x = 1:2: [NO] = [NO_2] = 250 ppm. [NH_3] = 500 ppm, 5 vol % H_2O, 5 vol % O_2, balance N_2, and GHSV = 400 000 h^{-1}.

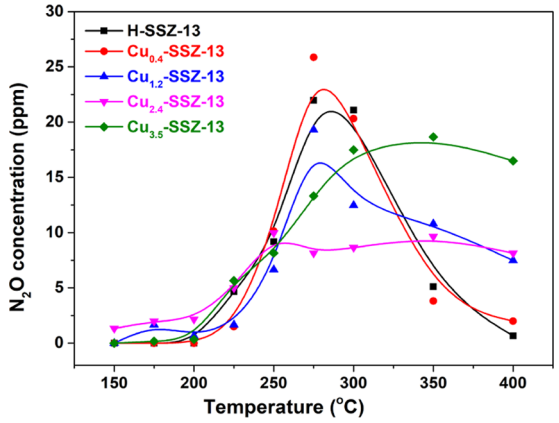

Figure 7. N_2O yields of NH_3-SCR under fast SCR conditions over H−SSZ-13 and Cu−SSZ-13 catalysts with different Cu loadings. Conditions: [NO] = [NO_2] = 250 ppm. [NH_3] = 500 ppm, 5 vol % H_2O, 5 vol % O_2, balance N_2, and GHSV = 400 000 h^{-1}.

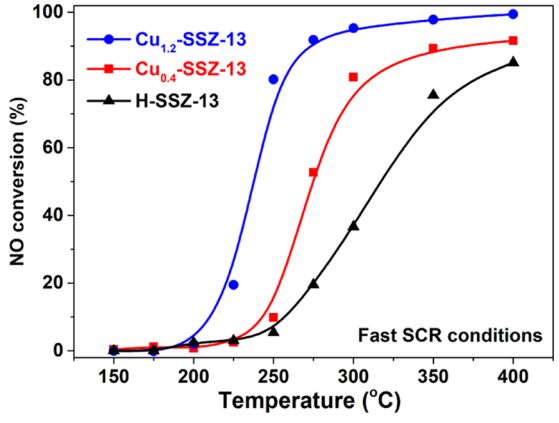

Figure 8. NO conversion under fast SCR conditions over H−SSZ-13, $Cu_{0.4}$−SSZ-13, and $Cu_{1.2}$−SSZ-13 catalysts. Conditions: [NO] = [NO_2] = 250 ppm. [NH_3] = 500 ppm, 5 vol % H_2O, 5 vol % O_2, balance N_2, and GHSV = 400 000 h^{-1}.

exchange with NH_4NO_3 solutions of different concentrations. The elemental analysis, Brunauer−Emmett−Teller (BET) surface areas, and micropore volume results for the products are listed in Table 1. The Cu loadings were varied from 3.5 to 0 wt % with approximately equal Si/Al ratios of 4 to 5. All of

DOI: 10.1021/acs.jpcc.8b05930
J. Phys. Chem. C 2018, 122, 25948−25953

Figure 9. Structural model and channel opening of the CHA framework.

the samples showed BET surface areas from 554.5 to 602.5 m^2/g with a micropore volume of ~0.24 cm^3/g, indicating that the zeolite structure was stable during the ion-exchange process and that ion-exchanged Cu ions did not block the zeolite pores appreciably. Figure 1 shows the XRD patterns of Cu−SSZ-13 catalysts, and all samples exhibited the typical diffraction peaks of the chabazite (CHA) zeolite structure with pure phase and a high degree of crystallinity, indicating that the CHA zeolite structure of one-pot-synthesized Cu−SSZ-13 was stable after ion exchange. H_2-TPR profiles of Cu−SSZ-13 catalysts with different Cu loadings are illustrated in Figure 2. No H_2 consumption was observed for H−SSZ-13, which means that all H_2 consumption peaks in the H_2-TPR profiles of Cu−SSZ-13 were due to the reduction of Cu species. As shown in Figure 2, $Cu_{0.4}$−SSZ-13 and $Cu_{1.2}$−SSZ-13 show a single H_2 consumption peak at around 350 °C, while the $Cu_{3.5}$−SSZ-13 and $Cu_{2.4}$−SSZ-13 samples with higher Cu loadings exhibit an additional peak at around 190 °C and 220 °C, respectively. According to previous studies,[4,23,29] the H_2 consumption peaks at around 190 °C and 220 °C can be assigned to the reduction of Cu^{2+} in the large CHA cages, and the H_2 consumption peak at around 350 °C can be assigned to the reduction of Cu^{2+} in the six-membered rings. However, it was found that the increase in the amount of H_2 consumption for the $Cu_{3.5}$−SSZ-13 catalyst was much higher than expected when compared to that for the $Cu_{2.4}$−SSZ-13 catalyst, if all Cu species in $Cu_{3.5}$−SSZ-13 existed only as Cu^{2+} ions. This indicates that besides the Cu^{2+} ions, the reduction of CuO_x clusters also contributes to the H_2 consumption peaks in the range 190−220 °C for the $Cu_{3.5}$−SSZ-13 catalyst.

3.2. NH_3-SCR Performance of Cu−SSZ-13. Figure 3 shows the NO and NO_2 conversion activities in the NH_3-SCR reaction for Cu−SSZ-13 catalysts with different Cu loadings in the temperature range from 150 to 400 °C under standard (NO_2/NO_x = 0) and fast (NO_2/NO_x = 1:2) SCR conditions. As was mentioned in the discussion on H_2-TPR profiles, with increasing Cu content, more Cu^{2+} species occupied the large cages of CHA, in which Cu^{2+} species were more active for the standard SCR reaction, since it was easier for Cu^{2+} to come in contact with reactants and to be reduced. This meant that Cu−SSZ-13 with more Cu^{2+} species in the large cages of CHA would show higher NO conversion at low temperatures. Therefore, the $Cu_{3.5}$−SSZ-13 and $Cu_{2.4}$−SSZ-13 catalysts, which contained Cu^{2+} species in the large cages of the CHA structure, showed higher NO conversion under standard SCR conditions, especially at low temperatures.

As shown in Figure 3, compared to the results under standard SCR conditions, the NO conversion under fast SCR conditions was totally inhibited at low temperatures below 225 °C. For all Cu−SSZ-13 series catalysts, no NO conversion was observed, meaning that at low temperatures, the fast SCR reaction pathway in which both NO and NO_2 should be involved in the reaction was inhibited over the Cu−SSZ-13 catalysts. This was consistent with what we have previously proved:[20] NH_4NO_3, formed from the NO_2 and NH_3 reaction, blocked the catalyst pores, leading to low NO conversion activity. It should also be noted that if we calculated the NO_x conversion under fast SCR conditions, the effect of NO_2 on the NO_x conversion activity changed from promotion to inhibition with increasing Cu loading, as shown in Figure 4. Additionally, the promotion effect became weaker and the inhibition effect become stronger with increasing Cu content. Therefore, the Cu species significantly influence NH_3-SCR performance under standard and fast SCR conditions.

However, when increasing the temperature further, a significant increase of NO conversion can be observed under fast SCR conditions because of the decomposition of NH_4NO_3. Interestingly, the NO conversion under fast SCR conditions was higher than that under standard SCR conditions for the $Cu_{0.4}$−SSZ-13 and $Cu_{1.2}$−SSZ-13 catalysts, demonstrating that besides reacting at Cu^{2+} sites, NO must also be reduced by NH_3 through another pathway when NO_2 is introduced; this was hypothesized to be the fast SCR pathway, as proved in the next section.

Figure 5 shows the TPSR profiles after NO_2 and NH_3 adsorption. The formation of surface NH_4NO_3 from the adsorbed NO_2 and NH_3 is a common reaction in the fast SCR reaction at low temperatures on Fe zeolites and Cu zeolites, according to the reaction below[30−32]

$$2NO_2 + 2NH_3 \rightarrow N_2 + NH_4NO_3 + H_2O \quad (3)$$

Many articles have shown that N_2O is released from the decomposition of NH_4NO_3 by the reaction[6,7]

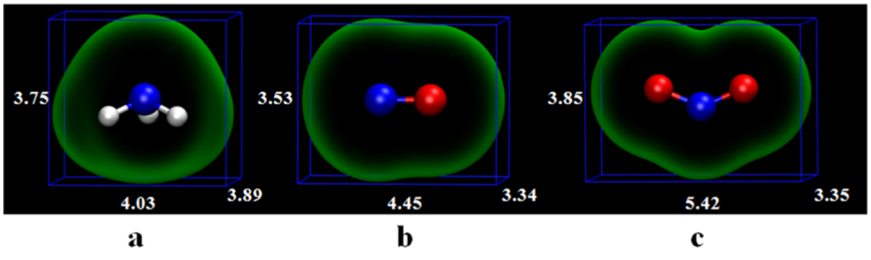

Figure 10. Molecular size defined by the electron density isosurface (isovalue = 0.0015 au). (a) NH_3, (b) NO, and (c) NO_2. The blue, red, and white circles denote N, O, and H atoms, respectively.

DOI: 10.1021/acs.jpcc.8b05930
J. Phys. Chem. C 2018, 122, 25948−25953

$$NH_4NO_3 \rightarrow N_2O + 2H_2O \quad (4)$$

As shown in Figure 5, the N_2O release temperature for the Cu−SSZ-13 catalysts was around 225 °C, which was exactly the cross-over temperature distinguishing the inhibition and promotion effects of NO_2 on the NO reduction, as shown in Figure 3. Therefore, the TPSR result also provided evidence for the formation of NH_4NO_3 on the fresh samples, which blocked the pores and decreased the NO conversion.

For the NO_2 conversion, the activity decreased with increasing Cu loading before the formed NH_4NO_3 decomposed. However, when the temperature was above 225 °C and after NH_4NO_3 had decomposed, the NO_2 conversion increased and leveled off at 100% with increasing Cu loading.

3.3. NH_3-SCR Performance of H−SSZ-13. For comparison, the NO and NO_2 conversion activities in the NH_3-SCR reaction of H−SSZ-13 were also evaluated, as shown in Figure 6. Under the standard SCR conditions, little NO conversion was observed, indicating that NO primarily reacted at Cu active sites. However, under the fast SCR conditions, although little NO conversion was observed, NO_2 conversion was noticeable, indicating that NO_2 could react with NH_3 at acid sites without the presence of Cu active sites at low temperatures.

In addition, at high temperatures above 250 °C, the NO conversion significantly increased despite the absence of Cu active sites, which was also observed on the $Cu_{0.4}$−SSZ-13 and $Cu_{1.2}$−SSZ-13 catalysts. Although the NH_4NO_3 decomposition at high temperatures led to recovery of some activity, the NO conversion under fast SCR conditions was higher than that under standard SCR conditions. This indicated that there existed another reaction pathway for NO when NO_2 was introduced.

Indeed, the reduction of ammonium nitrate by NO has been considered to be the rate-determining step of fast SCR.[10,30]

$$NH_4NO_3 + NO \rightarrow NO_2 + N_2 + 2H_2O \quad (5)$$

Therefore, deposited NH_4NO_3 could react with NO via reaction 5 rather than being removed by decomposition to N_2O on acid sites. As shown in Figure 7, the decrease in N_2O formation was observed on $Cu_{1.2}$−SSZ-13, $Cu_{0.4}$−SSZ-13, and H−SSZ-13 above 275 °C, demonstrating the weakened direct decomposition of NH_4NO_3 to N_2O. The combination of reactions 3 and 5 yields the fast SCR reaction 2, indicating that NO reduction will take place via the fast SCR reaction 2, which is likely to occur on acid sites. Also, this fast SCR reaction was hypothesized to be another pathway of NO_2 reduction by NH_3. However, it was found that Cu−SSZ-13 with high Cu loadings (2.4 and 3.5 wt %) showed no decrease in N_2O formation at temperatures above 275 °C, the reason for which is that NO was more active at Cu^{2+} sites compared to reacting with NH_4NO_3, therefore barely affecting the decomposition of NH_4NO_3 to N_2O. Moreover, the NO conversion levels over the H−SSZ-13, $Cu_{0.4}$−SSZ-13, and $Cu_{1.2}$−SSZ-13 catalysts under fast SCR conditions were compared, and the results are shown in Figure 8. The fast SCR reaction, involving NO and NO_2 conversion, occurred only at acid sites on H−SSZ-13. However, with the increasing Cu loading, NO conversion increased, indicating that NO conversion could also occur at Cu active sites on Cu−SSZ-13 catalysts.

3.4. Structure−Activity Relationships in NH_3-SCR Reaction. As the above results showed, NO_2 had a significant inhibition effect on NO conversion at low temperatures over the Cu−SSZ-13 catalysts, which was attributed to the formation of NH_4NO_3. However, for medium- and large-pore zeolites with the MFI and BEA structures, NH_4NO_3 formation also occurs, and little inhibition effect was observed over these catalysts because of the occurrence of fast SCR.[8,21,30,31] Chen et al.[31] found that small-pore Cu−CHA catalysts can stabilize NH_4NO_3 compared to Cu−BEA catalysts. However, before the decomposition of NH_4NO_3, the Cu zeolites with medium or large pores showed a NO_2 promotion effect on NO conversion.[8,14,21] Therefore, we here examined this mechanism from the aspects of zeolite geometry structure and reactant size.

Figure 9 shows that Cu−SSZ-13 catalysts are Cu-exchanged small-pore zeolites with the chabazite (CHA) crystal structure, which contain a channel opening of about 3.8 × 3.8 Å (an eight-membered ring).[31,33] The SCR reaction occurs when the reactants go through the channel opening (about 3.8 × 3.8 Å) and come in contact with the active sites. Figure 10 shows that the side lengths of rectangular boxes just enclosing the molecules are 3.75 × 3.89 × 4.03 Å, 3.34 × 3.53 × 4.45 Å, and 3.35 × 3.85 × 5.42 Å for NH_3, NO, and NO_2, respectively. Unlike NO, NH_3 and NO_2 exhibited geometric dimensions similar to the eight-membered ring. Therefore, the accumulation of NH_4NO_3 on the small pores led to heavy mass-transfer limitations, especially for NH_3 and NO_2. For MFI- and BEA-type zeolites (~5.3 × 5.6 Å and ~6.6 × 6.7 Å), however, the mass-transfer limitation was slight due to the large channel opening, resulting in fast SCR occurring at low temperatures.

Therefore, under fast SCR conditions, NH_3 and NO_2 were difficult to fit through the small pores at low temperatures when NH_4NO_3 formed. As a result, NO_2 and NH_3 primarily reacted at acid sites outside the zeolite cages, as was observed for the H−SSZ-13 samples, which showed a certain degree of NO_2 conversion. By contrast, no NO reduction was observed because of the absence of NH_3 at Cu active sites. After NH_4NO_3 decomposed at the temperature above 250 °C, the NO_2 conversion increased to 100% and leveled off. Meanwhile, the H−SSZ-13, $Cu_{0.4}$−SSZ-13, and $Cu_{1.2}$−SSZ-13 catalysts showed higher NO conversion activities under fast SCR conditions than those under standard SCR conditions, indicating that NO_2 addition had a promotion effect on NO conversion through the fast SCR reaction pathway.

4. CONCLUSIONS

The NH_3-SCR performances of small-pore Cu−SSZ-13 catalysts with varying Cu loadings were compared under standard and fast SCR conditions. It was found that increased Cu loadings contributed to standard SCR, while inhibited fast SCR. At low temperatures, the NO conversion activity was totally suppressed because of the formation of NH_4NO_3, while NO_2 could react with NH_3 at acid sites to contribute to NO_x conversion. The comparable geometric dimensions of the small pores and reactant molecules are responsible for the strong inhibition of the NO conversion activity by NO_2 addition. At high temperatures above 250 °C, when NH_4NO_3 decomposed, the fast SCR reaction occurred and resulted in the promotion of NO_x conversion, especially for Cu−SSZ-13 catalysts with low Cu loadings.

AUTHOR INFORMATION

Corresponding Author

*E-mail: honghe@rcees.ac.cn. Tel: +86 10 62849123.

DOI: 10.1021/acs.jpcc.8b05930
J. Phys. Chem. C 2018, 122, 25948−25953

ORCID

Yulong Shan: 0000-0002-5031-8522
Guangzhi He: 0000-0003-1770-3522
Yunbo Yu: 0000-0003-2935-0955

Notes

The authors declare no competing financial interest.

■ ACKNOWLEDGMENTS

This work was financially supported by the National Key R&D Program of China (2017YFC0211101), the National Natural Science Foundation of China (21637005, 51578536) and the K.C. Wong Education Foundation.

■ REFERENCES

(1) Kwak, J. H.; Tonkyn, R. G.; Kim, D. H.; Szanyi, J.; Peden, C. H. F. Excellent Activity and Selectivity of Cu−SSZ-13 in the Selective Catalytic Reduction of NOx with NH_3. *J. Catal.* **2010**, *275*, 187−190.

(2) Jo, D.; Ryu, T.; Park, G. T.; Kim, P. S.; Kim, C. H.; Nam, I.-S.; Hong, S. B. Synthesis of High-Silica LTA and UFI Zeolites and NH_3−SCR Performance of Their Copper-Exchanged Form. *ACS Catal.* **2016**, *6*, 2443−2447.

(3) Martín, N.; Paris, C.; Vennestrøm, P. N. R.; Thøgersen, J. R.; Moliner, M.; Corma, A. Cage-Based Small-Pore Catalysts for NH_3 -SCR Prepared by Combining Bulky Organic Structure Directing Agents with Modified Zeolites as Reagents. *Appl. Catal., B* **2017**, *217*, 125−136.

(4) Kim, Y. J.; Lee, J. K.; Min, K. M.; Hong, S. B.; Nam, I.-S.; Cho, B. K. Hydrothermal Stability of CuSSZ13 for Reducing NOx by NH_3. *J. Catal.* **2014**, *311*, 447−457.

(5) Zhang, T.; Qiu, F.; Li, J. Design and Synthesis of Core-Shell Structured Meso-Cu−SSZ-13@Mesoporous Aluminosilicate Catalyst for SCR of NOx with NH_3: Enhancement of Activity, Hydrothermal Stability and Propene Poisoning Resistance. *Appl. Catal., B* **2016**, *195*, 48−58.

(6) Devadas, M.; Krocher, O.; Elsener, M.; Wokaun, A.; Soger, N.; Pfeifer, M.; Demel, Y.; Mussmann, L. Influence of NO_2 on the Selective Catalytic Reduction of NO with Ammonia over Fe-ZSM5. *Appl. Catal., B* **2006**, *67*, 187−196.

(7) Grossale, A.; Nova, I.; Tronconi, E.; Chatterjee, D.; Weibel, M. NH_3−NO/NO_2 SCR for Diesel Exhausts Aftertreatment: Reactivity, Mechanism and Kinetic Modelling of Commercial Fe- and Cu-Promoted Zeolite Catalysts. *Top. Catal.* **2009**, *52*, 1837−1841.

(8) Shi, X.; Liu, F.; Xie, L.; Shan, W.; He, H. NH_3-SCR Performance of Fresh and Hydrothermally Aged Fe-ZSM-5 in Standard and Fast Selective Catalytic Reduction Reactions. *Environ. Sci. Technol.* **2013**, *47*, 3293−3298.

(9) Sjövall, H.; Blint, R. J.; Olsson, L. Detailed Kinetic Modeling of NH_3 SCR over Cu−ZSM-5. *Appl. Catal., B* **2009**, *92*, 138−153.

(10) Tronconi, E.; Nova, I.; Ciardelli, C.; Chatterjee, D.; Weibel, M. Redox Features in the Catalytic Mechanism of the "Standard" and "Fast" NH_3-SCR of NOx over a V-Based Catalyst Investigated by Dynamic Methods. *J. Catal.* **2007**, *245*, 1−10.

(11) Mao, Y.; Wang, Z.; Wang, H.-F.; Hu, P. Understanding Catalytic Reactions over Zeolites: A Density Functional Theory Study of Selective Catalytic Reduction of NOx by NH_3 over Cu−SAPO-34. *ACS Catal.* **2016**, *6*, 7882−7891.

(12) Wang, D.; Zhang, L.; Kamasamudram, K.; Epling, W. S. In Situ-Drifts Study of Selective Catalytic Reduction of NOx by NH_3 over Cu-Exchanged SAPO-34. *ACS Catal.* **2013**, *3*, 871−881.

(13) Janssens, T. V. W.; et al. A Consistent Reaction Scheme for the Selective Catalytic Reduction of Nitrogen Oxides with Ammonia. *ACS Catal.* **2015**, *5*, 2832−2845.

(14) Colombo, M.; Nova, I.; Tronconi, E. A Comparative Study of the NH_3-SCR Reactions over a Cu−Zeolite and a Fe-Zeolite Catalyst. *Catal. Today* **2010**, *151*, 223−230.

(15) Long, R. Q.; Yang, R. T. Reaction Mechanism of Selective Catalytic Reduction of NO with NH_3 over Fe-ZSM-5 Catalyst. *J. Catal.* **2002**, *207*, 224−231.

(16) Kwak, J. H.; Tran, D.; Szanyi, J.; Peden, C. H. F.; Lee, J. H. The Effect of Copper Loading on the Selective Catalytic Reduction of Nitric Oxide by Ammonia over Cu−SSZ-13. *Catal. Lett.* **2012**, *142*, 295−301.

(17) Koebel, M.; Elsener, M.; Madia, G. Reaction Pathways in the Selective Catalytic Reduction Process with NO and NO_2 at Low Temperatures. *Ind. Eng. Chem. Res.* **2001**, *40*, 52−59.

(18) Koebel, M.; Madia, G.; Elsener, M. Selective Catalytic Reduction of NO and NO_2 at Low Temperatures. *Catal. Today* **2002**, *73*, 239−247.

(19) Rahkamaa-Tolonen, K.; Maunula, T.; Lomma, M.; Huuhtanen, M.; Keiski, R. L. The Effect of NO_2 on the Activity of Fresh and Aged Zeolite Catalysts in the NH_3-SCR Reaction. *Catal. Today* **2005**, *100*, 217−222.

(20) Xie, L.; Liu, F.; Liu, K.; Shi, X.; He, H. Inhibitory Effect of NO_2 on the Selective Catalytic Reduction of NOx with NH_3 over One-Pot-Synthesized Cu−SSZ-13 Catalyst. *Catal. Sci. Technol.* **2014**, *4*, 1104−1110.

(21) Mihai, O.; Widyastuti, C.; Kumar, A.; Li, J.; Joshi, S.; Kamasamudram, K.; Currier, N.; Yezerets, A.; Olsson, L. The Effect of NO_2/NOx Feed Ratio on the NH_3-SCR System over Cu−Zeolites with Varying Copper Loading. *Catal. Lett.* **2014**, *144*, 70−80.

(22) Ren, L.; Zhu, L.; Yang, C.; Chen, Y.; Sun, Q.; Zhang, H.; Li, C.; Nawaz, F.; Meng, X.; Xiao, F. S. Designed Copper-Amine Complex as an Efficient Template for One-Pot Synthesis of Cu−SSZ-13 Zeolite with Excellent Activity for Selective Catalytic Reduction of NOx by NH_3. *Chem. Commun.* **2011**, *47*, 9789−9791.

(23) Xie, L.; Liu, F.; Ren, L.; Shi, X.; Xiao, F. S.; He, H. Excellent Performance of One-Pot Synthesized Cu−SSZ-13 Catalyst for the Selective Catalytic Reduction of NOx with NH_3. *Environ. Sci. Technol.* **2014**, *48*, 566−572.

(24) Mehio, N.; Dai, S.; Jiang, D. E. Quantum Mechanical Basis for Kinetic Diameters of Small Gaseous Molecules. *J. Phys. Chem. A* **2014**, *118*, 1150−1154.

(25) Zhao, Y.; Truhlar, D. G. The M06 Suite of Density Functionals for Main Group Thermochemistry, Thermochemical Kinetics, Noncovalent Interactions, Excited States, and Transition Elements: Two New Functionals and Systematic Testing of Four M06-Class Functionals and 12 Other Functionals. *Theor. Chem. Acc.* **2007**, *120*, 215−241.

(26) Frisch, M. J.; Trucks, G. W.; Schlegel, H. B.; Scuseria, G. E.; Robb, M. A.; Cheeseman, J. R.; Scalmani, G.; Barone, V.; Mennucci, B.; Petersson, G. A.; et al.*Gaussian 09*, revision D.01; Gaussian, Inc.: Wallingford, CT, 2009.

(27) Lu, T.; Chen, F. Multiwfn: A Multifunctional Wavefunction Analyzer. *J. Comput. Chem.* **2012**, *33*, 580−592.

(28) Humphrey, W.; Dalke, A.; Schulten, K. Vmd: Visual Molecular Dynamics. *J. Mol. Graph.* **1996**, *14*, 33−38.

(29) Hun Kwak, J.; Zhu, H.; Lee, J. H.; Peden, C. H.; Szanyi, J. Two Different Cationic Positions in Cu−SSZ-13? *Chem. Commun.* **2012**, *48*, 4758−4760.

(30) Iwasaki, M.; Shinjoh, H. A Comparative Study of "Standard", "Fast" and "NO_2" SCR Reactions over Fe/Zeolite Catalyst. *Appl. Catal., A* **2010**, *390*, 71−77.

(31) Chen, H.-Y.; Wei, Z.; Kollar, M.; Gao, F.; Wang, Y.; Szanyi, J.; Peden, C. H. F. A Comparative Study of N_2O Formation During the Selective Catalytic Reduction of NOx with NH_3 on Zeolite Supported Cu Catalysts. *J. Catal.* **2015**, *329*, 490−498.

(32) Grossale, A.; Nova, I.; Tronconi, E.; Chatterjee, D.; Weibel, M. The Chemistry of the NO/NO_2−NH_3 "Fast" SCR Reaction over Fe-ZSM5 Investigated by Transient Reaction Analysis. *J. Catal.* **2008**, *256*, 312−322.

(33) Kim, E.; Lee, T.; Kim, H.; Jung, W. J.; Han, D. Y.; Baik, H.; Choi, N.; Choi, J. Chemical Vapor Deposition on Chabazite (CHA) Zeolite Membranes for Effective Post-Combustion CO_2 Capture. *Environ. Sci. Technol.* **2014**, *48*, 14828−14836.

DOI: 10.1021/acs.jpcc.8b05930
J. Phys. Chem. C 2018, 122, 25948−25953